Vehicle agile maneuvering: From rally drivers to a finite state machine approach

Conference Paper · December 2016

DOI: 10.1109/SSCI.2016.7850095

3 authors:

Manuel Acosta Reche
Technische Universität Ilmenau
39 PUBLICATIONS **563** CITATIONS
SEE PROFILE

Stratis Kanarachos
Coventry University
199 PUBLICATIONS **2,030** CITATIONS
SEE PROFILE

Mike V Blundell
Coventry University
66 PUBLICATIONS **1,666** CITATIONS
SEE PROFILE

"Accepted subject to minor revisions, 2016 IEEE Symposium Series on Computational Intelligence ".

Vehicle agile maneuvering: From rally drivers to a finite state machine approach

Manuel Acosta
School of Mechanical, Aerospace and Automotive Engineering
Coventry University
United Kingdom
ac3354@coventry.co.uk

Stratis Kanarachos
School of Mechanical, Aerospace and Automotive Engineering
Coventry University
United Kingdom
ab8522@coventry.ac.uk

Mike Blundell
School of Mechanical, Aerospace and Automotive Engineering
Coventry University
United Kingdom
cex403@coventry.ac.uk

***Abstract*- Rally drivers can perform extreme vehicle maneuvers and keep a vehicle on track by maximizing the vehicle agility. It is remarkable that this is achieved robustly, without a vehicle or tire model in mind. In this study, the Moment Method Diagram and Beta Method representations are used to show the maximum achievable yaw moment generated by the front and rear tires. A new maneuverability map is proposed to bypass the limitations imposed by the steady state assumptions, based on the wheel slip – yaw moment representation. Furthermore, a simple driving automation strategy is developed to determine the sequence of inputs required for maximising vehicle agility and negotiating extreme maneuvers. A finite state machine is modelled and implemented using a two track vehicle model. The numerical results show that the finite state machine can resemble a rally driver.**

Keywords—agile maneuvering; autonomous driving; finite state machine; drift

I. INTRODUCTION

Agile maneuvering is conceived as the ability of the driver-vehicle interaction to generate important changes in vehicle attitude in a reduced amount of time. Normally, regular drivers drive from straight line to corners in quasi steady conditions [1], that is, with reduced yaw acceleration. Nevertheless, rally drivers are able to achieve high values of yaw acceleration to make fast transitions through reduced radius turns, e.g. Hairpin turns, thus using the full agility potential of the vehicle [2]. Due to the growing interest of the automotive industry in designing intelligent systems capable of operating autonomously and safely beyond the linear region limits, it is of vital important to understand how high yaw moments can be achieved [3,4].

In this paper, relevant background in agile maneuvering is presented. The most extended representations of vehicle handling (Milliken Moment Method [1] and Beta Method [5, 6]) are described to understand the full agility potential of the car and how to exploit it. Additionally, a new portrait (wheel slip – yaw Moment) is used to determine the combination of front and rear wheel slips required to generate a target yaw moment. Then, a finite state machine is implemented in a two track vehicle model (Matlab® / Simulink®) to drive the vehicle from straight line to cornering for different target yaw accelerations. Furthermore, in addition to the simulation results, metrics to characterize the vehicle agility are proposed (attitude change time (t_ψ), min sideslip (β) and max. yaw Acceleration ($\dot{r}$)). Conclusions and further steps are presented in the last section.

II. BACKGROUND

A. Agile maneuvering

Different approaches have been used to analyze agile maneuvering. Velenis, Tsiotras, Lu [7] studied the maneuvers commonly performed by Rally drivers (Trail braking and Pendulum turn) from an optimization perspective. Berntorp, Lundhal, Nielsen, Bernhardsson [8] found that in order to minimize the time to drive through a Hairpin turn, it is necessary to generate high sideslip angles (up to 40 deg). An important conclusion extracted from these works is that although the vehicle attitude is strongly dependent on the road grip, the vehicle trajectory remains almost invariant. This could benefit potential application of path following strategies in autonomous vehicles if the heading information is known in advance.

On the other hand, other authors have focused on analyzing the vehicle stability and controllability when operating with high sideslip angles (Drift equilibria). Edelmann, Ploch [9] used the root locus portrait to demonstrate that the drifting dynamics are highly unstable. Velenis, Katzourakis, Frazzoli, Tsiotras, Happee [10] implemented a LQR to stabilize the vehicle around a high sideslip solution and compare the results obtained from simulations and experimental data. Finally, Li, Zhang, Yi, Liu [11] studied the limits of the stable (sideslip-sideslip rate) area

for different control steering values. They proposed an extension of the boundaries of the "stable area" under the term "safe area", in which highly skilled drivers are able to operate and the full chassis potential is used.

B. *Moment Method diagram*

The Moment Method Diagram (MMD), *"Fig. 1"*, first appeared in the Milliken publication (Race Car Vehicle Dynamics [1]). It represents the lateral acceleration versus the normalized yaw moment (1) for different combinations of sideslip and steering angle.

$$C_N = \frac{N}{mg(l_f + l_r)} \tag{1}$$

The diagram is constructed by solving the planar dynamic equations for a given constant speed and assuming steady state conditions (zero sideslip rate). Overall, it provides valuable chassis information regarding grip limit, directional stability and maximum achievable yaw moment. A detailed description of this diagram as well as a study of the influence of different setup changes on the MMD shape is presented in [1]. Additionally, other works [12, 13] have intensively used this representation to evaluate vehicle stability and controllability.

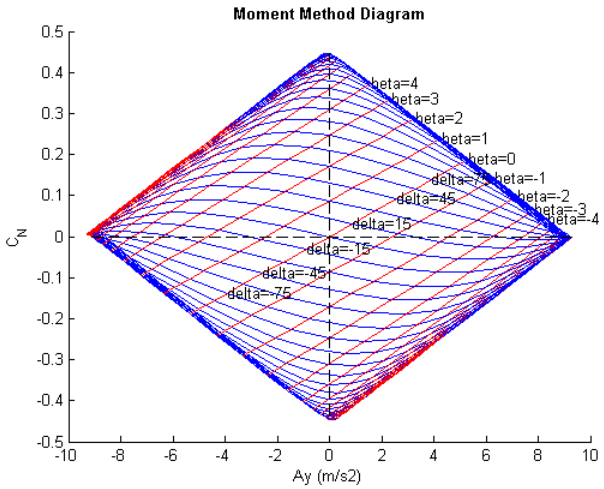

Fig. 1. MM Diagram generated with the parameters of "*Table I.*" at 80 kph.

The MMD presented above was generated using the vehicle parameters detailed in Table I. The ISO sign criterion was followed in this paper and the tire model is described in section III. In this case, the vehicle exhibits a slight understeer tendency at the limit (recovering yaw moment) and a maximum lateral acceleration of 9.2 m/s2 approximately.

TABLE I. Vehicle parameters

Notation	Value	Unit	Notation	Value	Unit
l_f	1.25	$[m]$	I_z	2500	$[kgm^2]$
l_r	1.35	$[m]$	$k_{\varphi f}$	110000	$[Nm/^\circ]$
m	1500	$[kg]$	$k_{\varphi r}$	70000	$[Nm/^\circ]$
t_{wf}	1.5	$[m]$	h_{CoG}	0.5	$[m]$
t_{wr}	1.5	$[m]$	SR	15	[-]

The influence of the speed in the directional stability of the vehicle is observed in *"Fig. 2.a"* and *"Fig. 2.b"*. At moderate speeds (left), the slope of the constant steer angle lines is very pronounced, and any lateral perturbation will be counteracted by a stabilizing yaw moment. Conversely, at high speeds (right), the slope reduces considerably and very little stabilizing moment is expected under lateral perturbations. It is important to remark that the contribution of the downforce is neglected in this analysis (passenger car). Therefore, the envelope of the diagram is expected to maintain constant regardless of the speed.

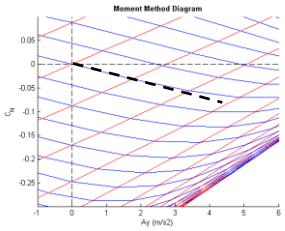

Fig. 2. a. Detail of MMD at 80 kph.

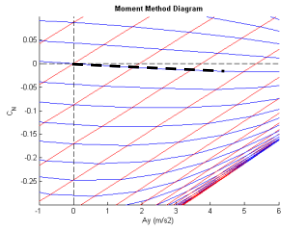

Fig. 2. b. Detail of MMD at 140 kph.

Finally, the diagram can be used to predict the vehicle states expected in a steady state maneuver. Thus, standard representations (sideslip - Ay), (steering angle - Ay) often used in chassis evaluation can be obtained for constant speed tests. E.g. "Slow increasing steer test" [1].

C. *Beta Method diagram*

The beta-method was developed by Shibahata, Shimada, Tomari [6] to study the influence of the vehicle sideslip angle on its maneuverability. This representation contains the same basic information as the MMD, but in this case the sideslip angle is plotted in the horizontal axis. This new axes layout facilitates the study of the relation between the sideslip and the remaining controllability (yaw moment) that can be used by the driver.

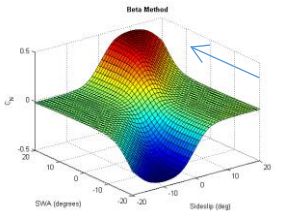

Fig. 3. a. 3D representation of the Beta diagram.

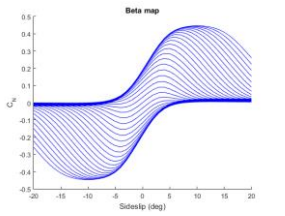

Fig. 3. b. 2D projection of the Beta diagram.

"Fig. 3.a" depicts schematically the axes transformation between the MMD and Beta Method. The normalized yaw moment (C_N) is plotted for each pair (δ, β) (left). The surface is

then projected on the beta – C_N axis, obtaining the Beta Method representation.

As pointed out by A. Zanten [5], the yaw moment available decreases dramatically when the sideslip angle is increased. It can be clearly appreciated in "Fig. 3.b" if the sideslip angle is augmented while the steering angle is maintained constant (moving in the steering angle isolines). Furthermore, it is important to notice that maximum yaw moment is achieved for combinations of steering and sideslip angle, not steering angle only.

To conclude, it can be understood from the work presented in this section that the yaw moment generated by the car will depend on the (δ, β) pair. In other words, the yaw moment with which the vehicle will start a maneuver from steady state conditions can be predicted if δ and β are known.

III. Description of the Vehicle Model

In this paper, a simplified two track model was constructed in (Matlab® / Simulink®) to evaluate the vehicle responses under different inputs. This section describes the planar dynamics, as well as lateral weight transfer, longitudinal weight transfer and tire model equations.

The numerical values of the vehicle parameters were listed in the previous section ("Table I").

A. Planar dynamics

The vehicle planar dynamics *("Fig 4"*) were modelled assuming negligible action of the pitch and roll dynamics over the yaw motion (2-4):

$$(\mathrm{F}_{x,1} + F_{x,2})\cos(\delta) - (F_{y,1} + F_{y,2})sin(\delta) + F_{x,3} + F_{x,4} = m(\dot{v_x} - v_y r) \quad (2)$$

$$(F_{y,1} + F_{y,2})\cos(\delta) + (\mathrm{F}_{x,1} + F_{x,2})\sin(\delta) + F_{y,3} + F_{y,4} = m(\dot{v_y} + v_x r) \quad (3)$$

$$((F_{y,1} + F_{y,2})\cos(\delta) + (\mathrm{F}_{x,1} + F_{x,2})\sin(\delta))l_f - (F_{y,3} + F_{y,4})l_r = I_z\dot{r} \quad (4)$$

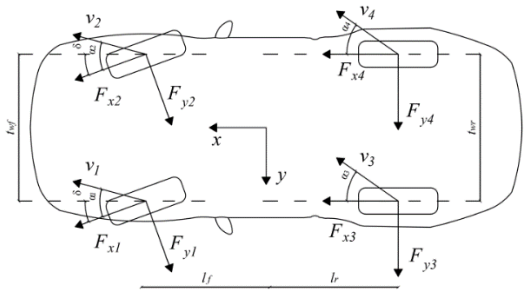

Fig. 4. Scheme of the planar dynamics model.

B. Kinematic equations

Wheel slips were calculated according to the following kinematic expressions (5-8):

$$\alpha_1 = \delta - \arctan\left(\frac{rl_f}{v_x - \frac{rt_{wf}}{2}} + \frac{v_y}{v_x}\right) \quad (5)$$

$$\alpha_2 = \delta - \arctan\left(\frac{rl_f}{v_x + \frac{rt_{wf}}{2}} + \frac{v_y}{v_x}\right) \quad (6)$$

$$\alpha_3 = -\arctan\left(-\frac{rl_r}{v_x - \frac{rt_{wr}}{2}} + \frac{v_y}{v_x}\right) \quad (7)$$

$$\alpha_4 = -\arctan\left(-\frac{rl_r}{v_x + \frac{rt_{wr}}{2}} + \frac{v_y}{v_x}\right) \quad (8)$$

In this paper, changes in wheel slip due to suspension compliances and/or bushings deflections are not considered. Furthermore, note that (5-8) can be simplified into the expressions (9-10) if the small angles assumption is taken and the term $\left(\frac{rt_w}{2}\right)$ is neglected.

$$\alpha_f = \delta - \left(\frac{rl_f}{v_x} + \frac{v_y}{v_x}\right) \quad (9)$$

$$\alpha_r = -\left(-\frac{rl_r}{v_x} + \frac{v_y}{v_x}\right) \quad (10)$$

C. Weight transfer

Vertical loads are calculated considering longitudinal and lateral weight transfer (11-13). For simplicity, only weight transfer through springs is taken into account (dampers are not modelled). Additionally, the roll center is considered to lie on the ground.

$$\mathrm{F}_{z,i} = \frac{mgl_j}{2WB} \mp \Delta F_{z,long} \mp \Delta F_{z,latj} \quad i \in \{1,2,3,4\}, j \in \{f,r\} \quad (11)$$

$$\Delta F_{z,long} = \frac{mh_{CoG}}{2WB} a_x \quad (12)$$

$$\Delta F_{z,latj} = \frac{mh_{CoG}}{t_{wj}}\left(\frac{k_{\varphi j}}{k_{\varphi f} + k_{\varphi r}}\right) a_y, \qquad j \in \{f,r\} \quad (13)$$

D. Tire model

Tires were modelled using the Pacejka Magic Formula, following a similar formulation than [8]. Equations (14-15) are used to compute the pure longitudinal and lateral forces. A weighting factor (16-21) is applied then to capture the effects of the interaction between longitudinal and lateral slips *("Fig 6"*).

$$\mathrm{F}_{x0,i} = \mu_{x,i} F_{z,i} \sin\left(C_{x,i}\, arctan\left(B_{x,i}\lambda_i - E_{x,i}\left(B_{x,i}\lambda_i - arctan\left(B_{x,i}\lambda_i\right)\right)\right)\right) \quad (14)$$

$$\mathrm{F}_{y0,i} = \mu_{y,i} F_{z,i} \sin\left(C_{y,i}\, arctan\left(B_{y,i}\alpha_i - E_{y,i}\left(B_{y,i}\alpha_i - arctan\left(B_{y,i}\alpha_i\right)\right)\right)\right) \quad (15)$$

$$H_{x\alpha,i} = B_{x1,i}\cos\left(arctan\left(B_{x2,i}\lambda_i\right)\right) \quad (16)$$

$$G_{x\alpha,i} = \cos\left(C_{x\alpha,i}\arctan\left(H_{x\alpha,i}\alpha_i\right)\right) \quad (17)$$

$$H_{y\lambda,i} = B_{y1,i}\cos\left(arctan\left(B_{y2,i}\alpha_i\right)\right) \quad (18)$$

$$G_{y\lambda,i} = \cos\left(C_{y\lambda,i}\arctan\left(H_{y\lambda,i}\lambda_i\right)\right) \quad (19)$$

$$F_{x,i} = F_{x0,i} G_{x\alpha,i}, \qquad i \in \{1,2,3,4\}, \quad (20)$$

$$F_{y,i} = F_{y0,i} G_{y\lambda,i}\,, \quad i \in \{1,2,3,4\}, \tag{21}$$

The tire parameters used in this work are listed in Table II, and were extracted from [8].

TABLE II. Tire model parameters

Notation	Front	Rear	Notation	Front	Rear
μ_x	1.2	1.2	μ_y	0.935	0.961
C_x	1.69	1.69	C_y	1.19	1.69
B_x	11.7	11.1	B_y	8.86	9.3
E_x	0.377	0.362	E_y	-1.21	-1.11
B_{x1}	12.4	12.4	B_{y1}	6.46	6.46
B_{x2}	-10.8	-10.8	B_{y2}	4.20	4.20
$C_{x\alpha}$	1.09	1.09	$C_{y\lambda}$	1.08	1.08

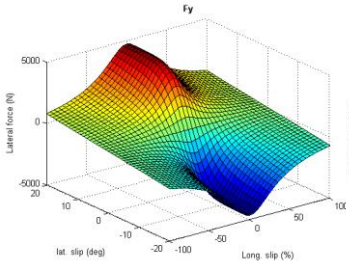

Fig. 5. a. Combined lateral force surface.

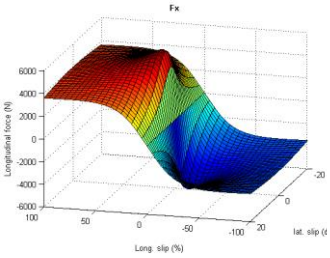

Fig. 5. b. Combined longitudinal force surface.

IV. Generating Maximum Yaw Moment

In section II the MMD and Beta Method representations were presented. As will be explained in this section, this portrays are fundamental to understand how the full agility of the vehicle can be exploit. *"Fig. 6"* illustrates two snapshots of a vehicle driving in straight line. In *"Fig 6.a"*, the vehicle sideslip is zero, being its velocity vector perfectly aligned with the tangent of the path. On the other hand, *"Fig 6.b"* shows a vehicle in which a positive sideslip angle has been induced.

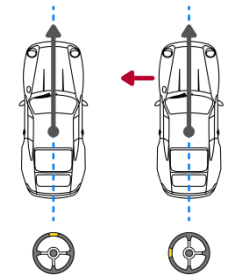

Fig. 6. a. Normal step input.

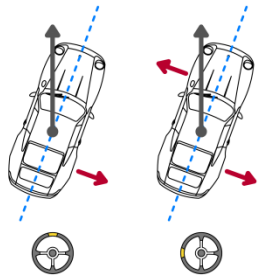

Fig. 6. b. Step input with sideslip angle.

For the purpose of this study it is considered that a sudden steering (δ) input is applied for negotiating a sharp left handed turn. Assuming that the steering input is fast enough (step shape), the yaw moment generated at each situation can be evaluated in the MMD, *"Fig. 7"*.

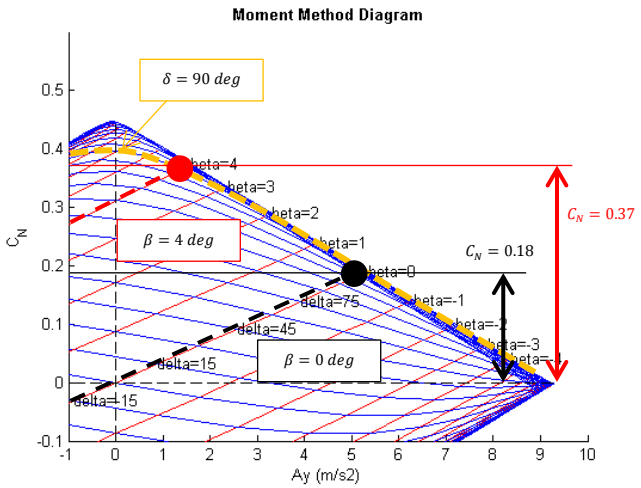

Fig. 7. Situations 6.a and 6.b illustrated in the MMD. Note the different in the yaw moment depending on the initial sideslip angle

As can be clearly appreciated in *"Fig. 7"*, the yaw moment generated in the second situation (positive sideslip) is considerably higher than the first situation. In fact, evaluating both representations, the high agility regions (max. yaw moment) can be achieved only for combinations of positive sideslip and steering input. The physical explanation of this phenomenon resides on the tire lateral forces.

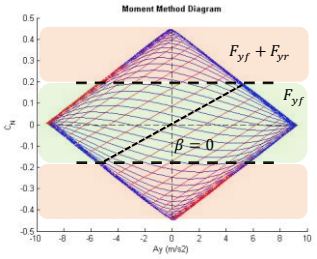

Fig. 8. a. MMD, regions of maximum yaw moment.

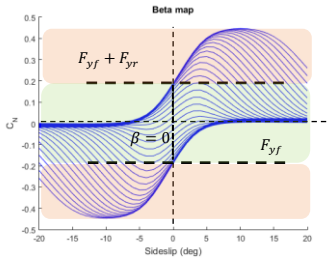

Fig. 18. b. Beta diagram, regions of maximum yaw moment.

In situation "b", it is achieved to drive the front and rear lateral forces out of phase. Thus, while the maximum yaw moment in situation "a" is limited by the front tires forces, the maximum yaw moment of situation "b" is created by both front and rear tires. "Fig. 8 a" and "Fig. 8 b" illustrate the limits of achievable yaw moment by the front tires (green shaded area) for zero sideslip.

This behavior (sideslip and steering input) can be noticed in motorsport Rally driving, when skilled drivers execute the Scandinavian Flick to change quickly the vehicle attitude in low grip conditions, trying to reduce the understeer of the vehicle.

Furthermore, results extracted from frequency response tests exhibit similar trends. When the steering input frequency approaches the minimum acceleration gain region (1-2 Hz), the front and rear wheel slips phase responses deviate until are out of phase.

A. *Limitations of the MMD (sideslip rate)*

From the previous sections, it is clear that there exist certain combinations of β and δ that permit achieving high yaw moments. Therefore, at this point one approach towards maximizing vehicle agility could be to use any of the described representations to determine the states required to reach maximum yaw moment. Nevertheless, it must be mentioned that these representations are generated under the assumption of steady state conditions (or in other words, considering null sideslip rate).

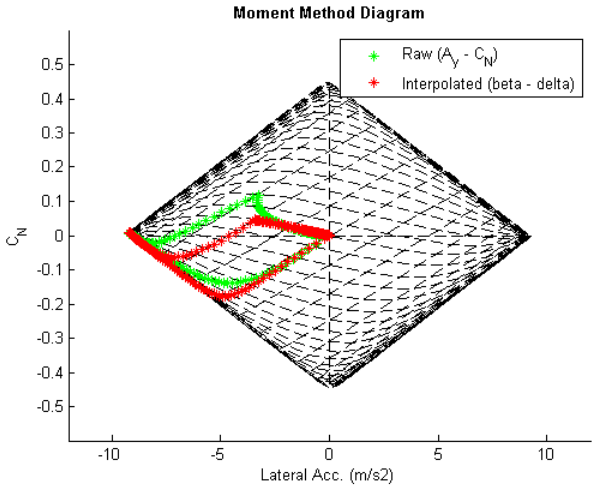

Fig. 9. Raw data from simulation and interpolated trajectories on the MMD.

In *"Fig. 9"*, two trajectories are plotted in the MMD. Both trajectories correspond to the same maneuver (Simulated Sine with Dwell), however the green trace is formed by graphing $(A_y - C_N)$ points while the red one contains interpolated $(\delta - \beta)$ points.

The trajectories differ considerably in the diagram due to the high transient content of the maneuver. For this reason, if the yaw moment is to be predicted from the vehicle states an alternative representation is necessary.

B. *Maneuverability map*

In this paper, the wheel slip versus yaw moment diagram is proposed as a robust maneuverability map. According to (eq. 4) and under the assumption of small steering angles, the yaw moment depends only on the lateral forces. These last are function of the longitudinal wheel slip, vertical forces and lateral wheel slips (eq. 9-10). Therefore, for each combination of (α_f, α_r) there exist a yaw moment, regardless of the sideslip rate. *"Fig. 10"* shows schematically the construction of the maneuverability map.

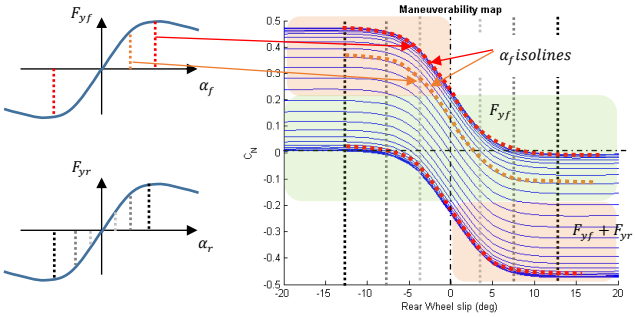

Fig. 10. Construction of the maneuverability map.

"Fig.11 a-b" represents the diagram for different values of longitudinal and lateral weight transfer. No influence of the lateral weight transfer is expected from the tire model used (lateral – vertical force proportionality, (14-15)).

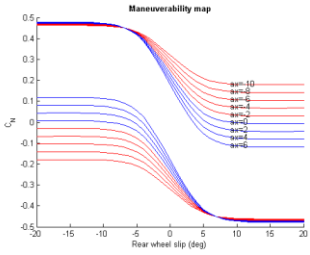

Fig. 11. a. Influence of long. Weight transfer.

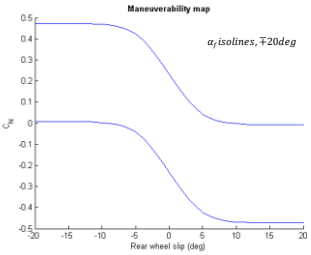

Fig. 11. b. Influence of lat. Weight transfer.

"Fig. 12 a-b" depicts the maneuverability map for different values of front and rear longitudinal slip. Expectedly, both front and rear longitudinal slips reduce the maximum achievable yaw moment due to the reduction of the available lateral forces. Finally, the road grip "scales" the map, reducing the total controllability area in low grip situations.

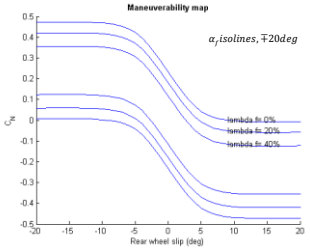

Fig. 12. a. Influence of front long. slip.

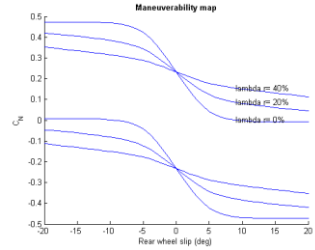

Fig. 12. b. Influence of rear long. slip.

Although the longitudinal slip and longitudinal weight transfer are coupled, authors decided to separate them to facilitate the evaluation of each individually. The principle of superposition could be applied to draw the map by adding these effects.

V. FINITE STATE MACHINE

A. Description of the Finite State Machine

The Finite State Machine proposed in this paper consists of three states *("Fig. 13")*. State 1 corresponds to the vehicle driving in straight line at constant speed, prior to start the maneuver. When a target yaw moment (M_{zref}) is given to the machine, the State can change to State 2 or State 3.

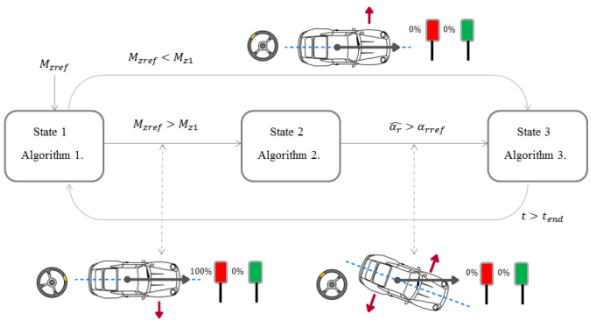

Fig. 13. State diagram of the Finite State Machine.

If M_{zref} is higher than the threshold M_{z1}, the machine switchs to State 2. If not, the machine goes directly to State 3. In State 2, the machine applies the steering and braking actions required to reach the rear wheel slip condition (α_r) necessary to achieve M_{zref}. Finally, when the sideslip condition is satisfactory, the machine switches to State 3, and the second steering input is applied to generate M_{zref}.

B. State 1 (Yaw moment Threshold)

The moment threshold $M_{z1}$is equal to the maximum yaw moment that can be generated with the front tires only ($\approx F_{yf} l_f$). The reference moment is evaluated in the Algorithm 1, expressed as follows:

Algorithm 1:

If $\{abs(M_{zref}) < M_{z1}\}$:

$\alpha_r = 0, \delta = SR(\alpha_{fref}), \lambda_f = 0, \lambda_r = 0,$

State=State 3

Else {}:

$\alpha_r = \alpha_{rref}, \delta = -\delta_1 sign(M_{zref}), \lambda_f = 0, \lambda_r = -1,$

State=State 2

Where the wheel slips (α_r, α_f) are calculated from the maneuverability map *"Fig. 15. a"*. The amplitude of the steering input δ_1 is determined from interpolation of the values showed in the look up table, Table 4.

TABLE IV. First input (δ_1) look up table

v\α_{rref}	5	10	15
60	60	70	75
80	55	60	65
100	50	55	60
120	50	55	55

The look up table is generated through simulation. The rear wheels are locked ($\lambda_r = -1$) and steering steps of increasing amplitudes are applied at different speeds. The time to reach different target rear wheel slips (t_{5r}, t_{10r}, t_{15r}) is saved. As can be observed in the surface of *"Fig.16 a"*, t_{10r} decreases considerably with the steering amplitude. *"Fig 16. b"* shows t_{5r} for different rear longitudinal slips. Expectedly, the time is minimized when the rear wheels are fully locked, which justifies $\lambda_r = -1$ condition.

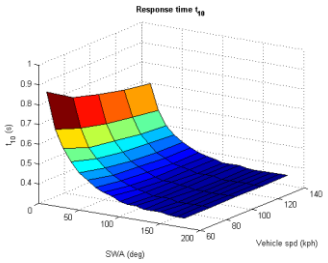

Fig. 14. a. Response time surface.

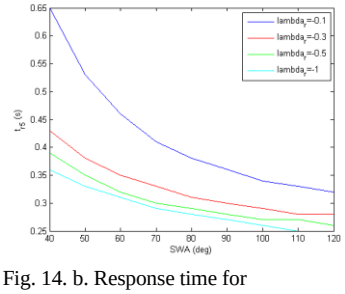

Fig. 14. b. Response time for different rear long. Slip (λ_r)

In order to keep δ_1 within reasonable values, the steering amplitude is selected as the value that crosses the 2% band of the minimum time. This condition is expressed by (22):

$$\delta_1 = \delta(1.02 \min(t_{\alpha r})) \quad (22)$$

C. State 2 (Sideslip build up)

Once State 2 is initiated, the Algorithm 2 is activated:

Algorithm 2:

If $\{abs(\widehat{\alpha_r}) < abs(\alpha_{rref})\}$:

$\delta = \delta_1, \lambda_f = 0, \lambda_r = -1,$

State=State 2

Else {}:

$\delta = \delta_2 sign(M_{zref}), \lambda_f = 0, \lambda_r = 0,$

State=State 3

Where the rear wheel slip ($\widehat{\alpha_r}$) is estimated from the expressions (23-24): and the steering input $\delta_2$is calculated using the kinematic relationship (25):

$$\widehat{v_y} = \int a_y - r v_x \tag{23}$$

$$\widehat{\alpha_r} = -\left(-\frac{r l_r}{v_x} + \frac{\widehat{v_y}}{v_x}\right) \tag{24}$$

$$\delta = SR\left(\alpha_{fref} + \frac{r l_f}{v_x} + \frac{\widehat{v_y}}{v_x}\right) \tag{25}$$

D. *State 3 (Return to straight line)*

Finally, the Machine returns to State 1 when the time condition t_{end} is surpassed.

Algorithm 3:
If $\{t < t_{end}\}$:
$hold\ \delta, \lambda_f = 0, \lambda_r = 0,$
State=State 3

Else {}:
$\delta = 0, \lambda_f = 0, \lambda_r = 0,$
State=State 1

VI. RESULTS

This section is intended to demonstrate the resemblance between the behavior of the state machine proposed in this paper and the Rally driving techniques employed when high yaw accelerations are required. In order to simplify the analysis, constant speed conditions are assumed, thus neglecting the effects of the rear wheel locking and induced drag in the longitudinal dynamics. Future works will consider these effects.

A. *Target yaw Moment Sweep*

First of all, several simulations were performed increasing the target yaw moment in several steps. In *"Fig. 15 a"* can be seen how the machine starts switching to the intermediate State 2 when the target yaw moment is higher than 8KNm. *"Fig. 15 b"* illustrates the time histories of the yaw moment values obtained in the simulation.

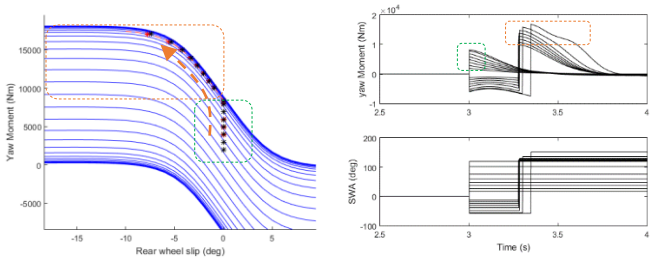

Fig. 15. a. Target yaw moment tracking.

Fig. 15. b. Yaw moment time histories.

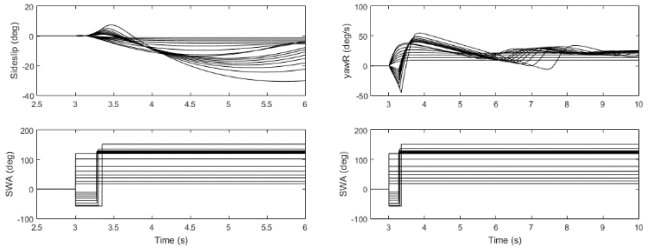

Fig. 16. a. Sideslip angle time histories.

Fig. 16. b. Yaw rate time histories.

Sideslip and yaw rate time histories are presented in *"Fig. 16 a"* and *"Fig. 16 b"* respectively. Notice how the maximum sideslip increases considerably with the target yaw moment.

B. *Maximum yaw acceleration*

Now, consider the following common situation in Rally driving. The driver is about to negotiate a 90 deg left turn and he desires to rotate the vehicle quickly, in order to align its heading angle with the exit straight and go back to the throttle earlier, achieving higher exit speed [14]. Two scenarios are considered:

In the first situation, *"Fig. 17 a"*, the driver applies a step input and generates the maximum yaw moment derived from the front tires (only steering input).

In the second situation, *"Fig. 17 b"*, the state machine applies the same steering input, but after going through State 2 (sideslip + steering input).

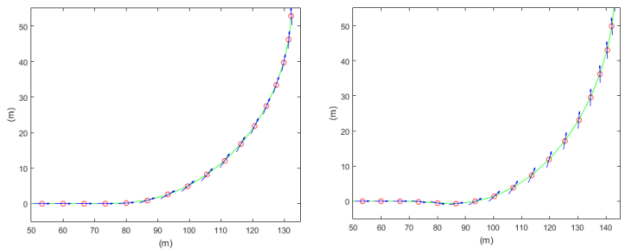

Fig. 17. a. Vehicle trajectory, normal Step.

Fig. 17. b. Vehicle trajectory, max. yaw moment strategy.

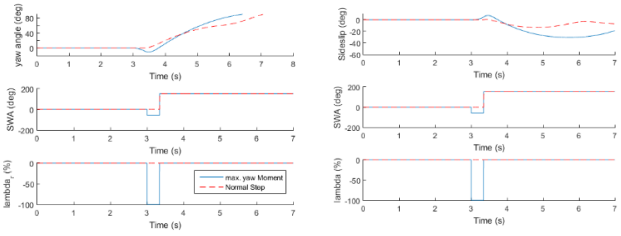

Fig. 18. a. Yaw angle time histories.

Fig. 18. b. Sideslip angle time histories.

As can be seen in *"Fig 18. a"*, the time to reach the 90 deg yaw condition is considerably lower (0.7s) when the max. yaw moment strategy is applied. Once the vehicle has been rotated, the driver can apply full throttle earlier and benefit from higher exit speed.

TABLE V. Agility metrics

Notation	Normal Step strategy	Max yaw Acc. strategy	Unit
$\dot{r}_{max}$	197	384	$[°/s^2]$
$t_{\Psi 90}$	3.7	3.0	$[s]$
β_{min}	-13.4	-30.3	$[°]$
$\dot{\beta}_{min}$	-16.6	-35.5	$[°/s]$

Table. V presents a comparison of the maximum yaw acceleration ($\dot{r}_{max}$), time to rotate the vehicle ($t_{\psi 90}$), minimum sideslip (β_{min}) and minimum sideslip rate ($\dot{\beta}_{min}$). Numerical values confirm that in order to maximize vehicle yaw acceleration and provoke high sideslip angles it is necessary to apply a high yaw moment strategy.

VII. CONCLUSIONS

In this paper a new approach towards agile maneuvering has been proposed. Using widely recognized vehicle handling representations it has been demonstrated that in order to maximize vehicle agility it is necessary to combine steering inputs with sideslip angles. This explains why Rally drivers excite the yaw dynamics when they approach hairpin turns in maneuvers such as Scandinavian Flick.

Furthermore, a Finite State Machine has been developed to perform autonomously the inputs required to reach high yaw acceleration regions. Results demonstrated that the sequence of input executed by the State Machine resemble skilled driver actions when the vehicle attitude is to be rotated fast.

Finally, it is intended that future works will increase the complexity of the proposed algorithms to handle successfully more complicated situations.

ACKNOWLEDGMENT

"This project has received funding from the European Union's Horizon 2020 research and innovation programme under the Marie Skłodowska-Curie grant agreement No 675999"

REFERENCES

[1] W.F.Milliken, D.L.Milliken, "Race Car Vehicle Dynamics",SAE International, 1995.

[2] M.Blundell, D.Harty, "The Multibody Systems Approach to Vehicle Dynamics", ElSevier, 2014.

[3] S. Kanarachos, M. Blundell and A. Kanarachos, "Minimum vehicle slip path planning for automated driving using a direct element method", Proceedings of the Institution of Mechanical Engineers, Part D: Journal of Automobile Engineering, 2015.

[4] S. Kanarachos, M. Alirezaei, S. Jansen and J. Maurice, "Control allocation for regenerative braking of electric vehicles with an electric motor at the front axle using the state-dependent Riccati equation control technique", Proceedings of the Institution of Mechanical Engineers, Part D: Journal of Automobile Engineering, vol. 228, no. 2, pp. 129-143, 2013.

[5] A Zanten. "Evolution of electronic control systems for improving the vehicle dynamic behavior." *Proceedings of the 6th International Symposium on Advanced Vehicle Control*. 2002.

[6] Y. Shibahata, K. Shimada, T. Tomari, "Improvement of Vehicle Maneuverability by Direct Yaw Moment Control", in *Vehicle System Dynamics*, 22 (1993), pp. 465 – 481.

[7] E. Velenis, P. Tsiotras and J. Lu, "Modeling aggressive maneuvers on loose surfaces: The cases of Trail-Braking and Pendulum-Turn," *Control Conference (ECC), 2007 European*, Kos, 2007, pp. 1233-1240.

[8] K. Berntorp, K. Lundhal, L. Nielsen, B. Bernhardsson, "Models and Methodology for Optimal Vehicle Maneuvers Applied to a Hairpin Turn", *American Control Conference (ACC)*, 2013.

[9] J. Edelmann, M. Plöchl, "Handling characteristics and stability of the steady-state powerslide motion of an automobile", *Regular and Chaotic Dynamics*, Vol. 14, No. 6. (1 December 2009), pp. 682-692.

[10] E. Velenis, D. Katzourakis, E. Frazzoli, P. Tsiotras, R. Happee, "Steady-state drifting stabilization of RWD vehicles", *Control Engineering Practice*, Vol. 19, Issue 11, November 2011, pp 1363-1376.

[11] J. Li, Y. Zhang, J. Yi, Z.Liu, "Understading Agile Maneuver Driving Strategies Using Coupled Longitudinal / Lateral Vehicle Dynamics", *ASME 2011 Dynamic Systems and Control Conference*. 2011.

[12] D. Kang, J.L. Stein, R.C. Hoffman, L.S. Louca, K. Huh, "Implementing the Milliken Moment Method using Controlled Dynamic Simulation", *SAE Vehicle Dynamics and Simulation*, 2005, pp 93 – 100.

[13] R.C. Hoffman, J.L. Stein, R.C. Hoffman, L.S. Louca, K. Huh, "Using the Milliken Moment Method and Dynamic simulation to evaluate Vehicle Stability and controllability", *International Journal of Vehicle Design (IJVD)*, Vol. 48, No. 1/2, 2008.

[14] M.White, Measurement and Analysis of Rally Car Dynamics at High Attitude Angles, PhD Thesis, Cranfield University.